Beta Estradiol Receptor Modulates Liver Lipid and Ketone Metabolism

Debora Santos Rocha*[1,2], Eloisa Vilas-Boas[3], Everton L. Vogt[1,2], Mariana Pacheco Teixeira de Carvalho[1,2], Maiara I. C. Queiroz[1,2], Camille C. Caldeira da Silva[1,2], Alicia J. Kowaltowski[1,2]

[1.] Departamento de Bioquímica, Instituto de Química, Universidade de São Paulo, São Paulo, Brazil
[2.] Centro de Metabolismo CoMeta, Hospital Universitário, Universidade de São Paulo, São Paulo, Brazil
[3.] Departamento de Análises Clínicas e Toxicológicas, Faculdade de Ciências Farmacêuticas, Universidade de São Paulo, São Paulo, Brazil

Corresponding author: Debora Santos Rocha (debora.santosrocha@usp.br)

Word Count: 5658

Figures: 6

Tables: 1

ABSTRACT

Non-selective hormone replacement with estradiol improves metabolic homeostasis during menopause. However, this treatment is not recommended for individuals with genetic predisposition to hormone-responsive cancers. In contrast, selective activation of estrogen receptor beta (ERβ) has shown promising results, promoting antitumor effects and modulating metabolic outcomes, although mechanisms in which these changes occur remain poorly understood. We investigated the effects of ERβ activation using diarylpropionitrile (DPN), a selective ERβ agonist, in both an *in vivo* model of post menopause and *in vitro* models of metabolic overload. Female Wistar rats were submitted to ovariectomy (OVX) and later treated with DPN. ERβ agonist treatment recovered fasting glucose and lipid profiles, improved pancreatic islet morphology, and reduced retroperitoneal white adipose tissue. Serum ketone bodies and free fatty acids levels were also recovered to control levels, suggesting a modulation in liver lipid oxidation. To isolate the direct effects mechanistically, hepatocytes were submitted to nutrient overload and treated with DPN. *In vitro*, DPN also recovered ketone body secretion and promoted an increased dependence on complete fatty acid oxidation as well as decreased metabolic flexibility, as assessed by modulated extracellular flux analysis. Overall, these findings demonstrate a new role of ERβ in the modulation of hepatic lipid and ketone metabolism, with positive metabolic outcomes in estradiol-deficient animals.

Keywords: estradiol receptor beta; mitochondria; liver; metabolism; menopause; metabolic dysfunction-associated steatotic liver disease

INTRODUCTION

Estrogen signaling plays a central role not only in reproductive functions, but also in energy metabolism, stimulating insulin production and secretion in pancreatic beta cells, and improving peripheral insulin signaling in the adipose tissue, muscle, and liver [1,2]. Accordingly, the postmenopausal decrease in estradiol levels leads to several metabolic consequences, including increased risk of metabolic disease development. This is observed both in humans and in animal models of estrogen deficiency induced by ovariectomy or hypothalamic-pituitary-gonad axis modulation [3]. Estrogen deficiency also promotes the accumulation of visceral white adipose tissue, which strongly contributes toward circulating free fatty acid (FFA) overload [4,5]. Subsequently, chronically increased levels of FFA compromise postprandial muscle glucose uptake and promote decompensation of hepatic glucose production. Long term glucotoxicity and lipotoxicity affect endocrine pancreatic responses to energy demands, culminating in defective insulin production and secretion, worsening the already impaired peripheral tissue insulin sensitivity [6,7].

In this sense, it is reasonable to assume that hormone replacement therapy (HRT) with estradiol would promote metabolic benefits postmenopause. In fact, HRT modulates adipose tissue redistribution to an insulin-sensitive phenotype, increasing subcutaneous and decreasing visceral depots [8], in addition to attenuating the metabolic imbalance associated with type II diabetes [9,10]. However, non-selective activation of estradiol receptors (ERs) often only has transient benefits which wane over time, and displays risks such as increased incidence of hormone-responsive tumor development in patients with gynecological cancer predisposition [11,12].

Estradiol used in HRT activates the 3 main types of estrogen receptors: nuclear receptors alpha (ERα) and beta (ERβ) as well as membrane receptors (GPER). ERα and ERβ receptors trigger estrogen response element binding, modifying gene transcription and, consequently, protein synthesis. These genomic responses to estrogens occur within hours. Conversely, the activation of membrane receptors (GPER) leads to a rapid response, within seconds or minutes, modulating cytosolic signaling processes including calcium influx [13] and activation of PKA and PKC pathways [14].

Selective ERα activation attenuates energy imbalance, improves insulin sensitivity, changes white adipose tissue (WAT) phenotype and promotes WAT browning [2,15,16]. Selective ERβ activation results are still poorly characterized, although data also suggest changes in WAT storage patterns, shifting from visceral to subcutaneous predominance [15], as well as WAT browning, and insulin sensitivity improvements [17], such as enhanced glucose uptake in muscle fibers [18]. Mechanistically, these effects of ERb activation remain to be characterized.

In the liver, estradiol reduces the unbalanced accumulation of triacylglycerol, and consequently steatosis, while also reducing gluconeogenesis, results that are generally attributed to ERa activation, due to its relative high expression levels [19–21]. The selective activation of ERβ in female rodents is also capable of triggering responses in

hepatocytes, reducing adipogenesis and lipid accumulation [22]. If these effects are also observed under postmenopausal conditions remains to be determined.

Determining if selective ERb activation promotes metabolic changes postmenopause is of interest because, while ERα activation is associated with the development of hormone-dependent cancers [23], ERβ activation has been described to exert antitumor [24–26], cell cycle inhibitory [27], and antiangiogenic effects [23,28]. Considering this, it is reasonable to assume that selective modulation of ERβ would be a promising alternative therapeutic target for postmenopausal metabolic syndrome. Therefore, the aim of this paper is to describe the metabolic effects of selective beta estradiol receptor (ERβ) activation under postmenopausal conditions, with a focus on the liver as a central metabolic hub.

MATERIALS AND METHODS

Animals

Female Wistar rats were maintained in collective cages at controlled temperatures (23°C) with 12-12 h light/dark cycles and with *ad libitum* access to food/water. All procedures were conducted in accordance with the Ethical Principles of Animal Manipulation of the local animal ethics committee, under CEUA-IQ/USP protocol 244/2022, and according to the National Research Council Guide for the Care and Use of Laboratory Animals [29,30].

At 90 days of age, the animals were submitted to an ovariectomy protocol as described in the "Ovariectomy surgery" section. Fifteen days later, they began treatment with ERβ agonist diarylpropionitrile (DPN, 1 mg · kg^{-1} · day^{-1}, s.c.) or vehicle (sesame oil) for 15 days. Four groups were studied: sham surgery treated with vehicle (Vehicle); sham surgery treated with DPN (DPN); ovariectomized animals treated with vehicle (OVX vehicle); and ovariectomized animals treated with DPN (OVX DPN). The animals were observed for 30 days for their food intake, weight gain, and glucose tolerance test responses (described in the "Glucose tolerance test" section). At the endpoint, the animals were anesthetized and killed by hypovolemic shock with cardiac punction. Serum was obtained after total blood centrifugation and stored for further analysis. Retroperitoneal white adipose tissue (WATr), uteruses and livers were collected and weighted. WATr, pancreases, and livers were evaluated for their histological characteristics (see "Histology analysis" section). The liver was also used for mitochondria isolation; fresh mitochondria were used to measure oxygen consumption rates as described in the "Oxygen consumption assay" section.

Ovariectomy surgeries

90-day-old female Wistar rats were anesthetized (4% isoflurane for induction and 1.5 to 2% for maintenance) and monitored for their temperature, heartbeat, and ventilation rates. The rat was positioned in a ventral decubitus position, and an incision was made between the lower costal margin and the thigh, approximately 1 cm lateral

to the midline. The muscle wall was retracted to allow access to the abdominal cavity. The ovary was located within the adipose tissue and removed after ligation of the corresponding uterine tube by sectioning between the ligature and the ovary. The muscle and skin were then sutured, and the procedure was repeated on the contralateral side [31]. After surgery, the animals were monitored and treated with Tramadol (20 mg/kg) for analgesia. None of the animals presented pain or distress considering the Grimace evaluation scale [32] Sham surgery animals also underwent anesthesia, ovary exposure, and postoperative analgesia and monitoring, without the removal of the ovaries.

Glucose tolerance tests

The glucose tolerance test response was evaluated before the ovariectomy surgery (week 1); 15 days after surgery and before DPN treatment (week 3); and after 30 days of surgery and 15 days of treatment (week 5). The animals were submitted to 6 hours of food deprivation and basal glucose levels were registered. Glucose (1 g per kg of body weight) was diluted in isotonic saline solution (NaCl 0.9%) and injected intraperitoneally. Blood glucose levels were registered at 5, 15, 30, 60, 90, 120, and 180 minutes using a Roche Accu-Chek glucometer.

Histological analysis

WATr, pancreas, and liver tissues were fixed in buffered formalin, dehydrated with ethanol solutions (70 to 100 %), embedded in paraffin, sectioned, mounted on slides, deparaffinized, and stained with hematoxylin/eosin. Images were registered with an Axio Scan.Z1 slide scanner and analyzed using QuPath software.

Pancreases were evaluated as for islet morphology. The endocrine tissue was visually identified, and islets were circulated individually. The shape descriptor tool was used to measure size and circularity. Islets were divided into quartiles as small, medium, or large using the control group as a reference [33,34]

WATr was analyzed according to Palomäki *et al.* [35]. The software was trained using the “train pixel classifier” tool. The brush and expected size range were used as training inputs. The “create objects” tool was then used and cell-by-cell visual confirmation ensured the correct output compared to the original image. The “shape descriptors” tool was used to analyze average adipocyte areas (μm^2).

Liver histology was evaluated for macrovesicular steatosis, considering the non-stained area within the tissue (apart from the portal vein branch area). Positive areas for macrovesicular steatosis were described as a percentage of the total area, and interpreted as neutral lipid accumulation *in vivo* [36,37].

Biochemical serum analysis

Serum was obtained after whole blood coagulation and centrifugation for 20 minutes at 300 g. The supernatant was collected and stored at -20°C. Serum total

cholesterol, HDL, LDL, triglycerides, free fatty acids, and beta hydroxybutyrate were detected using commercial kits (LabTest®, FUJIFILM®, and Sigma Aldrich®). VLDL levels were calculated by subtracting the measured HDL and LDL cholesterol fractions from the total cholesterol. Sample preparation, dilution, and standard curve protocols were conducted according to manufacturer instructions.

Tissue glycogen and triglycerides

Samples were hydrolyzed with 30% KOH at 100°C. Glycogen was precipitated in 70% ethanol, washed with distilled water, and converted into glucose by exposure to 4 M HCl at 100°C. Glycogen levels were measured based on glucose quantities resulting from this hydrolysis process compared to a commercial standard glycogen sample (Sigma-Aldrich) previously hydrolyzed in HCl solution. Detection was performed using a commercial colorimetric glucose assay kit (LabTest®). Triacylglycerol was detected directly using a commercial kit (LabTest®). These were expressed as µg triglycerides per µg protein and mg glycogen per mg tissue.

Mitochondrial oxygen consumption measurements

The liver was chopped into small pieces, suspended in isolation buffer (250 mM sucrose, 10 mM Hepes, 1 mM EGTA, 1 mM EDTA, 1 mg/mL bovine serum albumin, pH 7.2, at 4°C), and manually homogenized using a Potter–Elvehjem tissue grinder. The suspension was centrifuged twice (800 g, 4°C, 4 min), and the pellet discharged. The supernatant was further centrifuged at 9000 g, 4°C for 10 min. The pellet was resuspended in resuspension buffer (300 mM sucrose, 10 mM HEPES, and 2 mM EGTA, pH 7.2) and centrifuged again (9000 g, 4°C, 10 min). The pellet was resuspended in 1 mL of resuspension buffer, and total protein was quantified using the Bradford method.

For respirometry assays, 250 µg or 50 µg protein (for CI or CII–linked respiration respectively) of isolated mitochondria were incubated in a buffer containing 120 mM sucrose, 65 mM KCl, 2 mM $MgCl_2$, 1 mM KH_2PO_4, 1 mM EGTA, 10 mM HEPES, and 0.1% fatty acid-free BSA, pH 7.2, at 37°C in an Oroboros O2k high-resolution respirometer (Innsbruck, Austria). 1 mM pyruvate plus 1 mM malate and 1 mM α-KG, or 1 mM succinate plus 1 µM rotenone were used to induce CI-linked and CII-linked oxygen consumption, respectively. Oxygen consumption was monitored through sequential additions of ADP (1 mM) to induce state 3, oligomycin (1 µM) to induce state 4, and CCCP (titrated in 100 nM additions) for state 3u, as described in previous studies [38].

Cell cultures

Alpha mouse liver 12 cells (AML12, ATCC® CRL-2254™), a non-tumor cell line, were cultivated in Dubelco's modified Eagle's minimal essential medium (DMEM) (GIBCO®, Life Technologies) - low glucose concentration (5.6 mM) - supplemented with 10% fetal bovine serum (FBS), and 1% antibiotic-antifungal solution (Microlab®), without Phenol Red. The cells were kept in a humidified incubator at 37°C, in an atmosphere of 5% CO_2 and 95% air.

AML12 cells were plated and, after 24 hours, when they reached ~80% confluence, the medium was replaced with treatment medium lacking fetal bovine serum. The experimental groups were as follows: low glucose-BSA (LGB), high glucose-palmitate (HGP), and HGP plus ERβ agonist (DPN at doses of 0.1 nM or 1 nM for additional 24 h). The LGB group received bovine serum albumin (BSA, 0.25%) plus low glucose concentration (5.6 mM). The HGP group was exposed to BSA-Palmitate (200 µM) plus high glucose (20 mM).

Fluorescence microscopies

24 h after treatment, mitochondrial morphology was verified in cell cultures through live 3D fluorescence microscopy. Cells were loaded with Mitotracker Deep Red (50 nM) and BODIPY (1 µM) for 20 minutes. The media was then replaced by PBS, and images of live cells were taken using a Leica DMi8 fluorescence microscope [39]. The mitochondrial network was analyzed using the Mitochondrial Analyzer plugin (ImageJ software) and evaluated for mean volume and sphericity. Lipid droplets were assessed for their count and area per cell. 40 to 50 cells were quantified per group for each biological replicate. At least 5 different captured images were analyzed per biological replicate (n = 5).

Mitostress tests

After treatment, cells were washed in PBS twice and incubated in DMEM containing 5.6 mM glucose, 1% penicillin/streptomycin, and 5 mM Hepes, without FBS or bicarbonate. Oxygen consumption rates (OCR) were quantified using an extracellular flux analyzer (Seahorse XF24). Basal respiration was registered, and mitochondrial modulators were injected sequentially to quantify ATP-linked, maximal, and non-mitochondrial respiration by injecting oligomycin (1 µM), CCCP (1 µM), and antimycin plus rotenone (1 µM each), respectively. All mitochondrial modulators were titrated separately in preliminary experiments under LGB and HGP conditions (due to the potential quenching effect of fatty acids), and the doses used are the minimal required for a maximal response [38].

Metabolic flexibility assays

After treatment, cells were washed in PBS twice and incubated in DMEM containing 5.6 mM glucose, 1% penicillin/streptomycin, and 5 mM Hepes, without FBS or bicarbonate. Oxygen consumption rates (OCR) were quantified using an extracellular flux analyzer (Seahorse XF24). In the metabolic flexibility assay, cells were sequentially submitted to specific oxidation pathway inhibitors: Etomoxir (7 µM, a CPT1/FFA oxidation inhibitor), BPTES (glutaminase/GSL1 inhibitor - 8 µM), and UK5099 (mitochondrial pyruvate transporter inhibitor - 6 µM). A decrease in OCR after the inhibitor injection indicates the dependence on the specific substrate (when only this pathway is inhibited), and the maximum capacity to oxidize the specific substrate is obtained when the alternative pathways are inhibited. From this data, metabolic flexibility was calculated as the difference between dependence and capacity, indicating

cell effectiveness in substrate use changes. All the concentrations used were previously titrated under LGB and HGP conditions, as described above.

Western blots

Cells were homogenized in a RIPA buffer containing 50 mM HEPES, 40 mM NaCl, 50 mM NaF, 2 mM EDTA, 10 mM sodium pyrophosphate, 10 mM sodium glycerophosphate, 2 mM sodium orthovanadate, 1% Triton-X 100, and protease inhibitors without EDTA, then centrifuged at 13,000 rpm for 10 minutes at 4°C. Lysates were diluted in Laemmli buffer, and proteins were separated using a 10% denaturing polyacrylamide gel. Proteins were transferred to nitrocellulose membranes and incubated with specific antibodies (**Table 1**). Secondary antibodies were added for visualization of the bands, which were semi-quantified using densitometric analysis with Image J.

Statistical analysis

Data were evaluated using ANOVA test and Tukey posttest, when data presented gaussian distribution and variance homogeneity or correlate test for non-gaussian distribution. For animal data, two-way (OVX and DPN variables) unpaired tests were used to compare different individuals, while repeated measures analyses were applied to compare the same individual over time. For *in vitro* data, one-way paired tests were conducted since each biological replicate was divided across all experimental conditions. Also unpaired data are displayed as individual dots, and paired analyses are plotted as continuous lines connecting individual experiments. Significance was considered for differences when the p value was lower than 0.05.

RESULTS

ERβ agonist DPN modulates in vivo glucose homeostasis in ovariectomized (OVX) animals

The experimental design is shown in **Figure 1A**. The *in vivo* metabolic effects of OVX were monitored in female rats over the course of five weeks, in which Week 1 data were under baseline conditions, before the intervention protocol began; ERβ agonist (DPN) treatment began 15 days later, at Week 3. Measurements included body weight (BW), serum glucose levels, and glucose tolerance tests (GTT), repeated in Week 3 (15 days after the OVX surgery, prior to DPN treatment) and Week 5 (30 days after surgery and at 15 days of DPN treatment), when animals were euthanized and tissue analysis was conducted.

Figure 1B shows that OVX decreases endpoint uterus weights, as expected, with no noticeable effect of DPN. Weight gain over time (**Figure 1C**) was observed in all groups, and was significantly higher in OVX groups, as expected, with no significant effect of DPN. OVX slightly increased weight gain per calorie ingested, also with no effect of DPN (**Figure 1D**).

Glucose tolerance test (GTT) profiles before treatments at Week 1 (**Figure 1E**, area under the curve, and **Figure 1I**, basal glucose) were similar for all groups, indicating appropriate individual distribution prior to interventions. At Week 3, 15 days after OVX, but prior to DPN treatment, GTT areas under the curve (**Figure 1F**) and basal glucose levels (**Figure 1J**) were significantly higher in OVX animals, indicating the expected disrupted glucose metabolism. Interestingly, the loss of adequate responses to glucose overload in the GTT test promoted by OVX at Week 3 was not present at Week 5 (**Figure 1G**), although basal glucose levels were still significantly elevated in OVX animals relative to controls (**Figure 1K**). DPN promoted an increase in basal glucose levels in control animals, but significantly decreased the elevated basal glucose levels observed in OVX rats, reverting them to control levels. This indicates the ERβ agonist promotes significant glycemic control in OVX animals.

Given these effects on glucose homeostasis, we also examined endocrine pancreas histology (**Figure 1H**). OVX promoted an increase in smaller islets (**Figure 1L**) and a decrease in islet circularity (**Figure 1M**). DPN specifically increased islet size (**Figure 1L**) in the absence of OVX, while partially protecting against the decrease in circularity promoted by OVX (**Figure 1M**).

ERβ activation improves in vivo lipid homeostasis in OVX animals

The retroperitoneal white adipose tissue (WATr) was also evaluated in response to OVX and DPN (**Figure 2A**), given its importance as a metabolic hub. After treatment, as expected, OVX animals had significantly more WATr tissue, an effect that was abrogated by DPN treatment (**Figure 2B**). Interestingly, DPN also decreased average adipocyte areas in both control and OVX animals (**Figure 2C**).

In line with these anatomical adipose tissue findings, the serum lipid profile changed remarkably after OVX. Total cholesterol (**Figure 2D**, but not HDL, **Figure 2E**), LDL (**Figure 2F**), and VLDL (**Figure 2G**) were all increased by OVX, with strong protective effects of DPN on total (**Figure 2D**) and VLDL (**Figure 2G**) cholesterol levels. Serum triglycerides were also increased in OVX animals, in a manner prevented by DPN (**Figure 2H**). Serum non-esterified free fatty acid (NEFA) levels increased in OVX (**Figure 2I**), an effect accompanied by increased ketone bodies (**Figure 2J**). DPN treatment restored these parameters in OVX animals to the control levels (**Figures 2I** and **2J**). These results indicate that ERβ activation has protective effects against OVX-induced dyslipidemia and also promotes changes in lipid metabolism in the liver, from where ketone bodies are derived.

Post-OVX liver metabolism is modulated by selective ERβ activation

Due to its central function coordinating carbohydrate and lipid metabolism, along with the observed evidence of changes in liver-derived ketone bodies, the hepatic tissue was also evaluated. Histological (**Figure 3A**) and content analysis showed increased glycogen in OVX animals, an effect reversed by DPN (**Figure 3B**). Surprisingly, DPN had the opposite effect in non-OVX rats, increasing glycogen content in control animals (**Figure 3B**). Liver triglyceride content was also increased by OVX, but DPN

treatment did not alter this content significantly (**Figure 3C**). Consistently, macrovesicular steatosis was augmented by OVX, also with no effect of ERβ activation promoted by DPN (**Figure 3D**).

To further uncover changes in liver metabolism, flux analysis was performed by following oxygen consumption rates in freshly isolated liver mitochondria from the animals, using both Complex I-linked substrates (which generate NADH) and Complex II-linked succinate, which reduces FAD. Oxygen consumption rates were determined under state 3 conditions (with active oxidative phosphorylation) and state 4 conditions (in which ATP synthase and oxidative phosphorylation were inhibited by oligomycin, and oxygen consumption is proportional to the proton leak). With Complex I substrates, OVX increased both respiratory states, while respiration in mitochondria from OVX animals treated with DPN was equal to controls (**Figures 3E** and **3F**). Respiratory control ratios (RCR, state 3/state 4) were unchanged under all conditions (**Figure 3G**). Similar results were observed using Complex II-linked substrates, in which respiratory control ratios were equal, and both respiratory rates were increased by OVX, although the results were not reversed by DPN (**Figures 3H**, **3I**, and **3J**).

Selective ERβ activation modulates hepatocyte lipid metabolism

Overall, the results in the animals suggest that OVX promotes large metabolic modifications, resulting in marked unfavorable changes in circulating lipids and liver-derived ketones, which were prevented by DPN. While changes in liver were observed in animals, the hepatic storage of lipids was not fully reversed by DPN, and could not explain the serological effects of the drug alone. This could be due to alterations in mitochondrial metabolism *in situ* which depend on cytosolic signaling that are not conserved in isolated preparations. In order to overcome this limitation, we established a cell model using hepatocytes (AML-12 cells) in which the key metabolic features associated with OVX were mimicked by submitting the cells to high glucose combined with palmitate, and the effects of selective ERβ activation were verified by treatment with DPN (**Figure 4**).

Exposure of hepatocyte cells to a glucolipotoxic environment using high glucose and palmitate (HGP) led to the accumulation of lipid droplets (**Figure 4A-C**), in a manner unaffected by the presence of DPN, a result similar to that observed in the livers of OVX rats. Furthermore, HGP cells presented increased ketone secretion, in a manner prevented by two concentrations of DPN (**Figure 4D** and **4E**), once again mirroring effects seen in OVX animals. Thus, the HGP model presents similar effects to OVX and responds equally to ERβ activation, validating its use in uncovering mechanisms involved in this metabolic modulation.

Selective ERβ activation modulates in situ metabolic fluxes and targets regulatory checkpoints

Next, we conducted extracellular metabolic flux analysis in the hepatocyte cells using the Seahorse system, quantifying basal (**Figure 5A**), ATP-linked (**Figure 5B**), and

maximal (**Figure 5C**) oxygen consumption rates. All of these parameters were decreased in cells submitted to HGP relative to low glucose controls (LGB). Interestingly, ERβ activation with 0.1 nM or 1 nM DPN rescued these changes at least partially.

In order to uncover mechanisms for these changes, we quantified components of the oxidative phosphorylation machinery through western blot analysis (a typical blot is shown in **Figure 5D**). We found that Complexes I, II, III, IV, and V as well as inner mitochondrial membrane marker protein Tim 23 did not change in HGP condition, nor with DPN treatment (**Figure 5E-J**). Interestingly, DPN decreased Complex I protein levels (**Figure 5E**). Pyruvate dehydrogenase (PDH, **Figure 5K** and **5L**) levels were also decreased with DPN, a result that does not explain the increase in oxygen consumption rates promoted by this drug. When looking at other metabolic checkpoints, we found that HGP decreased both carnitine palmitoyltransferase 2 (CPT2, **Figure 5M**) and electron transfer flavoprotein subunit alpha (ETFA, **Figure 5N**) levels, showing that it affects components of fatty acid oxidation, in a manner that was not reversed by DPN. These results indicate that the changes in metabolic fluxes in the presence of DPN involve modulation of metabolic rates rather than control of the amounts of enzymes at the metabolic checkpoints involved.

ERβ selective activation modulates substrate dependence and metabolic flexibility in hepatocytes

Extracellular flux measurements can be designed to evaluate the participation of different metabolic pathways in intact cells, by following the effects of inhibitors of different metabolic pathways, alone or in combination. For that, we used UK5099, the mitochondrial pyruvate carrier inhibitor to specifically inhibit complete glucose oxidation (forming pyruvate, which enters mitochondria), Etomoxir (a carnitine palmitoyl transferase inhibitor) to prevent uptake of fatty acids into mitochondria, and BPTES, a glutaminase inhibitor, to assess the roles of carbohydrate, fatty acid, and amino acid oxidation on metabolic fluxes in hepatocytes (**Figure 6A**). By making sequential additions of the inhibitors alone or in combination, the dependence and capacity of each pathway can be assessed: <u>dependence</u> is evaluated by inhibiting the target pathway first, then the other pathways, while <u>capacity</u> is evaluated by inhibiting alternate pathways first, followed by the target pathway (**Figure 6A**). Finally, metabolic <u>flexibility</u> can be calculated as the difference between dependence and capacity. Experiments were done in parallel for two concentrations of DPN (0.1 and 1 nM) due to the number of samples needed, in order to conduct controls in parallel for the same sample.

Overall (**Figure 6B-S**), we found that nutrient overload with the high glucose and palmitate (HGP) protocol did not increase the capacity (panels **6C**, **6F**, **6I**, **6L**, **6O**, and **6R**) to oxidize pyruvate, glutamine, or palmitate relative to low glucose (LGB) conditions. Conversely, the dependence on the oxidation of glutamine (**Figures 6H** and **6K**) and pyruvate (**Figures 6B** and **6E**) increased under HGP conditions, leading to a condition of reduced metabolic flexibility (**Figures 6D**, **6G**, **6J** and **6M**). Interestingly, by significantly

increasing dependence (**Figures 6B**, **6E**, **6N** and **6Q**) on palmitate (**Figures 6P** and **6S**) and pyruvate (**Figures 6D** and **6G**), DPN further reduced flexibility on these substrates.

Together, these metabolic flux quantifications demonstrate that selective ERβ activation by DPN in hepatocytes promotes complete mitochondrial oxidation of carbohydrate-derived pyruvate and fat-derived palmitate, a result compatible with the fact that it decreases VLDL, triglycerides, fatty acids and ketones *in vivo*.

DISCUSSION

Estrogens promote growth and function of the reproductive tract, effects which can also be achieved in postmenopausal women by treatment with classical estrogen receptor agonists. Non-selective estrogen receptor agonists also have metabolic effects, at least partially reversing the undesirable metabolic impacts of menopause [8–10]. However, these beneficial results on metabolism are often unachievable in post-menopausal women who have predisposition toward hormone-responsive cancers, and therefore are not candidates for classic hormone replacement therapy. In this sense, it is of interest to understand the metabolic impact of selective ERβ activation, which is not associated with increased cancer risk [23–28]. Fittingly, we found that the *in vivo* treatment with the selective ERβ agonist DPN had no change in wet uterus weights, a result in line with existing literature suggesting that ERβ does not exert trophic effects on the reproductive organ in rodents [40,41], nor influence in the hypothalamic-pituitary-gonadal axis feedback [42].

A well-documented consequence of estradiol deficiency on energy metabolism is persistent weight gain, not always correlated with food intake [20,43,44]. Indeed, we find that OVX animals exhibited marked weight gain beginning in the first week post-ovariectomy, which remained pronounced until the experimental endpoint (30 days). Body weight gain per caloric intake was elevated in OVX animals, indicating increased energy conversion efficiency induced by estradiol deficiency. Selective ERb activation with DPN had no effect on body weight gain or weight gain relative to caloric intake in OVX animals, a finding consistent with a prior study showing that ERβ agonists do not significantly affect body weight [45].

Although the ERβ agonist did not influence body weight, marked changes were observed in glucose and lipid homeostasis after treatment was introduced post-OVX. OVX induced impairments in basal glucose levels, accompanied by changes in pancreatic islet size and circularity [7]. OVX also increased WATr weight and elevated serum cholesterol, LDL, VLDL, triglycerides, and fatty acids - confirming the establishment of an energy overload state induced by estradiol deficiency, characterized in previous literature by elevated fasting glucose, development of insulin resistance [20], increased white adipose tissue mass, and a disrupted circulating lipid profile [44]. DPN treatment did not alter the GTT profile, but restored basal glucose levels in OVX animals to those observed in controls. DPN also improved islet circularity, preserving physiological pancreatic islet morphology. Moreover, treatment with DPN decreased WATr weight and adipocyte areas in both control and OVX animals, accompanied by improvements in

serum cholesterol, VLDL, triglycerides, and FFAs. These data demonstrate that selective ERβ activation, even after estradiol deficiency establishment, can restore critical markers of metabolic disease risk, improving both glucose and lipid homeostasis, in many cases to levels indistinguishable from non-OVX controls.

The effects on glucose homeostasis and islet morphology suggest DPN may also exert direct actions on the endocrine pancreas. *In vitro* studies suggest that ERβ, along with ERα and GPER, enhances β-cell survival and function, with ERβ contributing toward apoptosis prevention and K_{ATP} inhibition mimicry [46,47]. ERβ$^{-/-}$ mice showed delayed first-phase insulin release following glucose stimulation, but with no changes in basal glucose levels [48]. Another study found that DPN did not significantly affect glucose or glycated hemoglobin (HbA1c) in OVX Sprague-Dawley rats [49]. Conversely, an ERβ agonist decreased serum glucose levels and improved β-cell function in high-fat diet-fed mice [50], so the direct effects of the receptor on b-cells seem to be dependent on the metabolic state and animal model.

Visceral adiposity reduction may explain the decreased FFAs promoted by DPN treatment observed in our *in vivo* model, as visceral fat exhibits high lipolytic activity, linked to a detrimental cardiovascular profile and β-cell dysfunction [51–53]. Indeed, ERβ activation may promote adipose tissue remodeling [45]. In male rats, ERβ agonist treatment shifted fat distribution from visceral to subcutaneous without affecting body weight - a pattern associated with reduced lipolytic activity and improved insulin sensitivity [45]. In OVX females, ERβ agonists prevented WAT gain, enhanced lean mass [54], reduced LDL, and improved hepatic insulin sensitivity under high-fat diet conditions [50]. We found that serum β-hydroxybutyrate levels followed the same pattern as FFAs - increased in OVX animals and fully restored to control levels after DPN treatment. As incomplete lipid oxidation to acetyl CoA is associated with hepatic ketone body production [55,56], these findings implicate the liver, alongside the adipose tissue and endocrine pancreas, in the beneficial metabolic effects observed with ERβ activation *in vivo.* Given the liver's central role in lipid metabolism, and the scarcity of ERβ-focused liver studies, we investigated hepatic metabolic status in OVX females.

We found that OVX induced significant changes in liver metabolism, with increased glycogen and lipid accumulation, suggesting substrate overload and enhanced storage signaling. Notably, the GTT curve did not differ between OVX and controls animals, suggesting preserved insulin sensitivity. However, increased ketone production alongside lipid accumulation suggests early-stage metabolic-associated fatty liver disease (MASLD)-like decompensation [57,58], although macrovesicular steatosis remained within physiological levels [59]. We also assessed mitochondrial function in freshly isolated liver mitochondria. Both state 3 (phosphorylating) and state 4 (proton-leak dependent) oxygen consumption were elevated in OVX animals, indicating higher electron transport rates and reduced coupling efficiency between oxygen consumption and ATP synthesis. This inefficiency is a known feature of estradiol deficiency and is recoverable via non-selective estradiol treatment [60,61], implicating estrogen receptors in mitochondrial regulation [61–63]. Fittingly, our results showed that DPN-treated OVX animals did not have

differences in mitochondrial oxygen consumption rates when compared to controls, indicating that the treatment restores these parameters of oxidative phosphorylation. These results are different from previously reported estradiol (non-selective) effects [61–63] and suggest ERβ may have distinct effects on mitochondrial respiration.

While ERβ mitochondrial effects in liver had not been uncovered previously, some work has shown that ERβ appears to be involved in hepatic lipid metabolism, and may attenuate MASLD progression [54,64], despite its lower expression levels [22,54] in this organ. Our findings indicate that OVX-induced lipid accumulation resulted and mild steatosis without structural liver damage, suggesting ongoing but subclinical metabolic imbalance, but without a change in liver triglycerides nor histological macrovesicular steatosis detection upon DPN treatment. This may be compatible with the improvement of serological factors, since the persistence of triglycerides can be a protective adaptation through proper esterification processes of free fatty acids, which would otherwise be toxic [65,66].

To understand the changes in metabolism happening in liver cells in terms of specific metabolic modulation, we also conducted *in vitro* studies. Our model reproduced the effects of nutrient overload seen *in vivo*, with accumulation of lipid droplets in hepatocytes and enhanced ketone release. As seen *in vivo*, DPN prevented ketone production [67,68], but not lipid accumulation. This indicates that ERβ activation can directly regulate FFA oxidation in hepatocytes, and that the prevention of ketone generation does not depend on systemic effects of the drug. Interestingly, the effects of DPN involve metabolic flux rewiring, with increased dependence and decreased flexibility of the full oxidation of carbohydrate-derived pyruvate and the fatty acid palmitate. This metabolic shift promoted by DPN, which favors full oxidation of acetyl-CoA, can explain the lower release of partially oxidized ketone products from lipids under conditions of nutrient overload.

Interestingly, estradiol enhances hepatic oxidative machinery and substrate oxidation [69,70], a result that is partially compatible with our results suggesting ERβ may reduce the capacity of these processes, while also increasing dependence on the full oxidation of pyruvate and fatty acids, with a decrease in metabolic flexibility. This indicates that ERβ activation promotes specific metabolic shifts in liver cells that impact on *in vivo* lipid and glucose metabolism, promoting improved systemic glucose and lipid homeostasis, despite persistent energy overloads seen in the absence of estrogens. These findings highlight ERβ as a promising alternative to non-selective estradiol therapy, particularly for postmenopausal individuals who face metabolic challenges.

FUNDING

This work was supported by the *Fundação de Amparo à Pesquisa do Estado de São Paulo* (FAPESP) under grant numbers 13/07937-8 (Centro de Pesquisa, Inovação e Difusão em Processos Redox, Redoxoma) , 2020/06970-5, 2021/04781-3, and 24/13461-0, as well as the *Conselho Nacional de Desenvolvimento Científico e Tecnológico* (CNPq) grants 408213/2024-8 (Metodologias Quantitativas e de Precisão em Biomedicina

Redox) and 303886/2021-8, as well as *Coordenação de Aperfeiçoamento de Pessoal de Nível Superior* (CAPES) line 001.

AUTHORS' RELATIONSHIPS AND ACTIVITIES

The authors declare that there are no relationships or activities that might bias, or be perceived to bias, their work.

ACKNOWLEDGEMENTS

The authors acknowledge Professor Vilma Regina Martins for intellectual contributions and discussions. We also thank Silvânia M. P. Neves and her animal facility crew for exceptional expert animal care and Sirley Mendes de Oliveira for excellent technical support. Finally, we acknowledge Mario Costa Cruz (CONFOCAL – CEFAP facility) for histological image capturing.

CONTRIBUTION STATEMENT

DSR is responsible for conception and design of research, under the supervision of AJK; EAVB contributed with experimental design suggestions; EAVB, ELV, MICQ, and CCCS performed *in vivo* experiments and analyzed data; MPTC performed *in vitro* experiments and analyzed data; DSR interpreted results and prepared figures; DSR and AJK drafted the manuscript; all authors revised and approved the final version of the manuscript. DSR is the guarantor of this work and, as such, had full access to all the data in the study and takes responsibility for the integrity of the data and the accuracy of the data analysis.

REFERENCES

1. Mahboobifard, F. *et al.* Estrogen as a key regulator of energy homeostasis and metabolic health. *Biomed Pharmacother* **156**, 113808 (2022).

2. Barros, R. P. A. & Gustafsson, J. Å. Estrogen receptors and the metabolic network. *Cell Metab* **14**, 289–99 (2011).

3. Cheng, Y. *et al.* Follicle-stimulating hormone orchestrates glucose-stimulated insulin secretion of pancreatic islets. *Nat Commun* **14**, 6991 (2023).

4. Poehlman, E. T., Toth, M. J. & Gardner, A. W. Changes in energy balance and body composition at menopause: A controlled longitudinal study. *Ann Intern Med* **123**, 673–675 (1995).

5. Lobo, R. A. Metabolic syndrome after menopause and the role of hormones. *Maturitas* **60**, 10–8 (2008).

6. Poitout, V. & Robertson, R. P. Glucolipotoxicity: Fuel excess and β-cell dysfunction. *Endocr Rev* **29**, 351–66 (2008).

7. Cerqueira, F. M. *et al.* Diluted serum from calorie-restricted animals promotes mitochondrial β-cell adaptations and protect against glucolipotoxicity. *FEBS J* **283**, 822–833 (2016).

8. Cox-York, K. A., Erickson, C. B., Pereira, R. I., Bessesen, D. H. & Van Pelt, R. E. Region-specific effects of oestradiol on adipose-derived stem cell differentiation in post-menopausal women. *J Cell Mol Med* **21**, 677–684 (2017).

9. Livingstone, C. & Collison, M. Sex steroids and insulin resistance. *Clin Sci* **102**, 151–166 (2002).

10. De Los Angeles Carrasco-Ruiz, M. *et al.* High estradiol differentially affects the expression of the glucose transporter type 4 in pelvic floor muscles of rats. *Int Neurourol J* **22**, 161–168 (2018).

11. Leitman, D. C. *et al.* Tissue-specific regulation of genes by estrogen receptors. *Semin Reprod Med* **30**, 14–22 (2012).

12. Cedó, L., Reddy, S. T., Mato, E., Blanco-Vaca, F. & Escolà-Gil, J. C. HDL and LDL: Potential New Players in Breast Cancer Development. *J Clin Med* **8**, 853 (2019).

13. Tesarik, J. & Mendoza, C. Nongenomic effects of 17 beta-estradiol on maturing human oocytes: relationship to oocyte developmental potential. *J Clin Endocrinol Metab* **80**, 1438–1443 (1995).

14. Kelly, M. J. & Wagner, E. J. Estrogen Modulation of G-protein-coupled Receptors. *Trends in Endocrinology & Metabolism* **10**, 369–374 (1999).

15. Musatov, S. *et al.* Silencing of estrogen receptor alpha in the ventromedial nucleus of hypothalamus leads to metabolic syndrome. *Proc Natl Acad Sci U S A* **104**, 2501–2506 (2007).

16. Barreto-Andrade, J. N. *et al.* Estrogen receptor 1 (ESR1) enhances Slc2a4/GLUT4 expression by a SP1 cooperative mechanism. *Int J Med Sci* **15**, 1320–1328 (2018).

17. González-Granillo, M. *et al.* Selective estrogen receptor (ER)β activation provokes a redistribution of fat mass and modifies hepatic triglyceride composition in obese male mice. *Mol Cell Endocrinol* **502**, 110672 (2020).

18. Barros, R. P. A., Machado, U. F., Warner, M. & Gustafsson, J.-A. Muscle GLUT4 regulation by estrogen receptors ERbeta and ERalpha. *Proc Natl Acad Sci U S A* **103**, 1605–1608 (2006).

19. Buniam, J., Chukijrungroat, N., Khamphaya, T., Weerachayaphorn, J. & Saengsirisuwan, V. Estrogen and voluntary exercise attenuate cardiometabolic syndrome and hepatic steatosis in ovariectomized rats fed a high-fat high-fructose diet. *Am J Physiol Endocrinol Metab* **316**, 908–921 (2019).

20. Bailey, C. J. & Ahmed-Sorour, H. Role of ovarian hormones in the long-term control of glucose homeostasis - Effects on insulin secretion. *Diabetologia* **19**, 475–81 (1980).

21. Gao, H., Fält, S., Sandelin, A., Gustafsson, J. Å. & Dahlman-Wright, K. Genome-wide identification of estrogen receptor α-binding sites in mouse liver. *Molecular Endocrinology* **22**, 10–22 (2008).

22. Foryst-Ludwig, A. *et al.* Metabolic Actions of Estrogen Receptor Beta (ERβ) are Mediated by a Negative Cross-Talk with PPARγ. *PLoS Genet* **4**, 1000108(2008).

23. Arnal, J. F. *et al.* From in vivo gene targeting of oestrogen receptors to optimization of their modulation in menopause. *Br J Pharmacol* **165**, 57–66 (2012).

24. Radde, B. N. *et al.* Bioenergetic differences between MCF-7 and T47D breast cancer cells and their regulation by oestradiol and tamoxifen. *Biochem J* **465**, 49–61 (2015).

25. Radde, B. N. *et al.* Nuclear respiratory factor-1 and bioenergetics in tamoxifen-resistant breast cancer cells. *Exp Cell Res* **347**, 222–231 (2016).

26. Salama, S. A. *et al.* Estradiol-17β upregulates pyruvate kinase M2 expression to coactivate estrogen receptor-α and to integrate metabolic reprogramming with the mitogenic response in endometrial cells. *J Clin Endocrinol Metab* **99**, 3790–3799 (2014).

27. Liao, T. L., Tzeng, C. R., Yu, C. L., Wang, Y. P. & Kao, S. H. Estrogen receptor-β in mitochondria: implications for mitochondrial bioenergetics and tumorigenesis. *Ann N Y Acad Sci* **1350**, 52–60 (2015).

28. Caruntu, C. *et al.* The role of estrogens and estrogen receptors in melanoma development and progression. *Acta Endocrinol (Copenh)* **12**, 234–241 (2016).

29. Leary, S., Underwood, W., Anthony, R. & Cartner, S. AVMA Guidelines for the Euthanasia of Animals: 2013 Edition. *American Veterinary Medical Association* (2013).

30. Council, N. R. *Guide for the Care and Use of Laboratory Animals: Eighth Edition*. *The National Academies Press* (2011).

31. Idris, A. I. Ovariectomy/orchidectomy in rodents. *Methods Mol Biol* **816**, 545–551 (2012).

32. Langford, D. J. *et al.* Coding of facial expressions of pain in the laboratory mouse. *Nat Methods* **7**, 447–449 (2010).

33. Munhoz, A. C. *et al.* Adiponectin reverses β-Cell damage and impaired insulin secretion induced by obesity. *Aging Cell* **22**, 13827 (2023).

34. Huang, S. *et al.* Increased CD34 in pancreatic islet negatively predict islet β-cell decrease in type1 diabetes model. *Front Physiol* **13**, 1032774 (2022).

35. Palomäki, V. A., Koivukangas, V., Meriläinen, S., Lehenkari, P. & Karttunen, T. J. A Straightforward Method for Adipocyte Size and Count Analysis Using Open-source Software QuPath. *Adipocyte* **11**, 99–107 (2022).

36. Brunt, E. M. Nonalcoholic steatohepatitis (NASH): Further expansion of this clinical entity? *Liver* **19**, 263–264 (1999).

37. Brown, G. T. & Kleiner, D. E. Histopathology of nonalcoholic fatty liver disease and nonalcoholic steatohepatitis. *Metabolism* **65**, 1080–1086 (2016).

38. Vilas-Boas, E. A., Cabral-Costa, J. V., Ramos, V. M., Caldeira da Silva, C. C. & Kowaltowski, A. J. Goldilocks calcium concentrations and the regulation of oxidative phosphorylation: Too much, too little, or just right. *J Biol Chem* **299**, 102904 (2023).

39. Kakimoto, P. A., Serna, J. D. C., de Miranda Ramos, V., Zorzano, A. & Kowaltowski, A. J. Increased glycolysis is an early consequence of palmitate lipotoxicity mediated by redox signaling. *Redox Biol* **45**, 102026 (2021).

40. Malamas, M. S. *et al.* Design and Synthesis of Aryl Diphenolic Azoles as Potent and Selective Estrogen Receptor-β Ligands. *J Med Chem* **47**, 5021–5040 (2004).

41. Mewshaw, R. E. *et al.* ERβ Ligands. 3. Exploiting Two Binding Orientations of the 2-Phenylnaphthalene Scaffold to Achieve ERβ Selectivity. *J Med Chem* **48**, 3953–3979 (2005).

42. Hewitt, S. C., Harrell, J. C. & Korach, K. S. Lessons in estrogen biology from knockout and transgenic animals. *Annual Review of Physiology* **67** 285–308 (2005).

43. D'Eon, T. M. *et al.* Estrogen Regulation of Adiposity and Fuel Partitioning: Evidence of Genomic and Non-Genomic Regulation of Lipogenic and Oxidative Pathways. *Journal of Biological Chemistry* **280**, 35983–35991 (2005).

44. Brown, L. M., Gent, L., Davis, K. & Clegg, D. J. Metabolic impact of sex hormones on obesity. *Brain Research* **1350**, 77–85 (2010).

45. González-Granillo, M. *et al.* Selective estrogen receptor (ER)β activation provokes a redistribution of fat mass and modifies hepatic triglyceride composition in obese male mice. *Mol Cell Endocrinol* **502**, 110672 (2020).

46. Babiloni-Chust, I. *et al.* G protein-coupled estrogen receptor activation by bisphenol-A disrupts the protection from apoptosis conferred by the estrogen receptors ERα and ERβ in pancreatic beta cells. *Environ Int* **164**, 107250 (2022).

47. Soriano, S. *et al.* Rapid Regulation of KATP Channel Activity by 17β-Estradiol in Pancreatic β-Cells Involves the Estrogen Receptor β and the Atrial Natriuretic Peptide Receptor. *Molecular Endocrinology* **23**, 1973–1982 (2009).

48. Barros, R. P. A., Gabbi, C., Morani, A., Warner, M. & Gustafsson, J. Å. Participation of ERα and ERβ in glucose homeostasis in skeletal muscle and white adipose tissue. *Am J Physiol Endocrinol Metab* **297**, 124-133 (2009).

49. Bansal, S. & Chopra, K. Distinct role of estrogen receptor-alpha and beta on postmenopausal diabetes-induced vascular dysfunction. *Gen Comp Endocrinol* **206**, 51–9 (2014).

50. González-Granillo, M. *et al.* ERβ activation in obesity improves whole body metabolism via adipose tissue function and enhanced mitochondria biogenesis. *Mol Cell Endocrinol* **479**, 147–158 (2019).

51. Lafontan, M. & Langin, D. Lipolysis and lipid mobilization in human adipose tissue. *Prog Lipid Res* **48**, 275–297 (2009).

52. Nielsen, S., Guo, Z., Johnson, C. M., Hensrud, D. D. & Jensen, M. D. Splanchnic lipolysis in human obesity. *J Clin Invest* **113**, 1582–1588 (2004).

53. Karastergiou, K., Smith, S. R., Greenberg, A. S. & Fried, S. K. Sex differences in human adipose tissues - The biology of pear shape. *Biology of Sex Differences* **3**, 13 (2012).

54. Yepuru, M. *et al.* Estrogen receptor-β-selective ligands alleviate high-fat diet- and ovariectomy-induced obesity in mice. *Journal of Biological Chemistry* **285**, 31292–31303 (2010).

55. ROSENBLOOM, J. The acetone bodies in diabetes mellitus: influence of low and high protein intake on the excretion of acetone, diacetic acid and beta-oxybutyric acid. *J Am Med Assoc* **65**, 1715–1717 (1915).

56. Nelson, A. B., Queathem, E. D., Puchalska, P. & Crawford, P. A. Metabolic Messengers: ketone bodies. *Nat Metab* **5**, 2062–2074 (2023).

57. Sunny, N. E., Parks, E. J., Browning, J. D. & Burgess, S. C. Excessive hepatic mitochondrial TCA cycle and gluconeogenesis in humans with nonalcoholic fatty liver disease. *Cell Metab* **14**, 804–810 (2011).

58. Lambert, J. E., Ramos-Roman, M. A., Browning, J. D. & Parks, E. J. Increased de novo lipogenesis is a distinct characteristic of individuals with nonalcoholic fatty liver disease. *Gastroenterology* **146**, 726–735 (2014).

59. Brown, G. T. & Kleiner, D. E. Histopathology of nonalcoholic fatty liver disease and nonalcoholic steatohepatitis. *Metabolism: Clinical and Experimental* **65**, 1080–1086 (2016).

60. Fuller, K. N. Z. *et al.* Estradiol treatment or modest exercise improves hepatic health and mitochondrial outcomes in female mice following ovariectomy. *Am J Physiol Endocrinol Metab* **320**, 1020–E1031 (2021).

61. Mattingly, K. A. *et al.* Estradiol stimulates transcription of nuclear respiratory factor-1 and increases mitochondrial biogenesis. *Molecular Endocrinology* **22**, 609–622 (2008).

62. Nilsen, J., Chen, S., Irwin, R. W., Iwamoto, S. J. & Brinton, R. D. Estrogen protects neuronal cells from amyloid beta-induced apoptosis via regulation of mitochondrial proteins and function. *BMC Neurosci* **7**, 1965–1970 (2006).

63. Gigli, I. & Bussmann, L. E. Exercise and Ovarian Steroid Hormones Their Effects on Mitochondrial Respiration. *Life Sciences* 68, 1505–1514 (2001).

64. Shin, E. S. *et al.* Genistein Downregulates SREBP-1 Regulated Gene Expression by Inhibiting Site-1 Protease Expression in HepG2 Cells 1,2. *The Journal of Nutrition Biochemical, Molecular, and Genetic Mechanisms J. Nutr* **137,** 1127–1131 (2007).

65. Listenberger, L. L. *et al.* Triglyceride Accumulation Protects against Fatty Acid-Induced Lipotoxicity. *Proc Natl Acad Sci U S A* 100, 3077–3082 (2003).

66. Ricchi, M. *et al.* Differential effect of oleic and palmitic acid on lipid accumulation and apoptosis in cultured hepatocytes. *Journal of Gastroenterology and Hepatology (Australia)* **24**, 830–840 (2009).

67. Martins-Maciel, E. R., Campos, L. B., Salgueiro-Pagadigorria, C. L., Bracht, A. & Ishii-Iwamoto, E. L. Raloxifene affects fatty acid oxidation in livers from ovariectomized rats by acting as a pro-oxidant agent. *Toxicol Lett* **217**, 82–89 (2013).

68. Weinstein, I., Soler-Argilaga, C., Werner, H. V & Heimberg, M. Effects of Ethynyloestradiol on the Metabolism of I1-V1CIOleate by Perfused Livers and Hepatocytes from Female Rats. *Biochem. J* **180**, 265–271 (1979).

69. Rettberg, J. R., Yao, J. & Brinton, R. D. Estrogen: A master regulator of bioenergetic systems in the brain and body. *Front Neuroendocrinol* **35**, 8–30 (2014).

70. Klinge, C. M. Estrogenic control of mitochondrial function and biogenesis. *Journal of Cellular Biochemistry* **105,** 1342–1351 (2008).

71. Technologies, A. *Agilent XF Substrate Oxidation Stress Test Kits User Manual*. (2020).

FIGURE LEGENDS

Figure 1. ERβ agonist modulates glucose homeostasis in ovariectomized (OVX) female Wistar rats. Experimental protocol (**A**). Uterus weight (**B**), body weight gain (**C**), final body weight gain per caloric intake (**D**). Week 1 (**E**), week 3 (**F**), and week 5 (**G**) GTT AUC. Week 1 (**H**), week 3 (**I**), and week 5 (**J**) basal glucose levels. Representative islet histology (**K**), pancreatic islet size distribution (**L**), pancreas circularity (**M**). Groups were compared by two-way ANOVA followed by Tukey posttest. Significances were considered at $p < 0.05$.

Figure 2. ERβ agonist modulates lipid homeostasis in ovariectomized (OVX) female Wistar rats. Representative WATr histology (**A**). Retroperitoneal white adipose tissue (WATr) weight (**B**), WATr adipocyte area (**C**), serum cholesterol (**D**), HDL (**E**), LDL (**F**), VLDL (**G**), triglycerides (**H**), non-esterified fatty acids (**I**), and β-hydroxybutyrate (**J**). Groups were compared by two-way ANOVA followed by Tukey posttest. Significances were considered at $p < 0.05$.

Figure 3. ERβ agonist modulates liver metabolism in ovariectomized (OVX) female Wistar rats. Representative liver histology (**A**), liver glycogen (**B**), triglycerides (**C**), and macrovesicular steatosis (**D**). Mitochondrial Complex I-linked State 3 (St3) oxygen consumption rates (**E**); Complex I-linked State 4 (St4) oxygen consumption rates (**F**); CI-linked Respiratory Control Ratio (RCR) (St3/St4) (**G**); mitochondrial Complex II-linked State 3 (St3) oxygen consumption rates (**H**); Complex II-linked State 4 (St4) oxygen consumption rates (**I**); CI-linked RCR (St3/St4) (**J**). Groups were compared by two-way ANOVA followed by Tukey posttest. Significances were considered at $p < 0.05$

Figure 4. ERβ agonist restores ketone body production without changes in lipid levels and mitochondrial morphology in hepatocytes submitted to energy overload. Representative images for mitochondrial network and lipid droplets using Mitotracker deep red (gray) and BODIPY (yellow) (**A**); lipid droplets count (**B**) and area (**C**) per cell; β-hydroxybutyrate release to culture medium after 24 h of treatment (**D** and **E**). Groups were compared by one-way ANOVA. Significances were considered at $p < 0.05$.

Figure 5. ERβ agonist effects on oxygen consumption, levels of mitochondrial oxidative phosphorylation components and metabolic checkpoints. Basal (**A**), ATP-linked (**B**), and maximal (**C**) oxygen consumption rates. Representative blot of oxidative phosphorylation components using total Oxphos antibody mix (**D**) using TIM23 as internal control. Quantification of protein levels of mitochondrial complexes I, II, III, IV and V (**E-J**). Representative blots (**K**) and quantifications of pyruvate dehydrogenase (PDH, **L**), Carnitine palmitoyltransferase II (CPT2, **M**), electron transfer flavoprotein subunit alpha (EFTA, **N**). Ponceau staining was used for normalization in L-M. Groups were compared by one-way ANOVA. Significances were considered at $p < 0.05$.

Figure 6. ERβ activation modulates substrate oxidation dependence and flexibility under conditions of energy overload. Oxygen consumption rates (OCR) were measured under basal conditions, and after the injection of 7 µM Etomoxir (CPT1 inhibitor), 6 µM UK5099 (mitochondrial pyruvate carrier inhibitor) and/or 8 µM BPTES (glutaminase

inhibitor), as indicated, to measure dependence and capacity [**Panel A**, adapted from Agilent [71], created with Biorender]. Capacity was measured after injecting all inhibitors except for the target oxidative pathway inhibitor. Dependence was expressed as the target substrate per all inhibitor response ratio. Capacity was expressed as the alternative substrates' response per all inhibitors' response ratio. Flexibility is the difference between the capacity and the dependence. Values were quantified for the different substrates, and using two DPN concentrations (**Panels B-M**). Groups were compared by one-way ANOVA. Significances were considered at $p < 0.05$.

TABLES

Table 1. Antibodies and dilutions

Target	Company	Code	Dilution
Mitochondrial complexes I-V	Abcam	110413	1:1000
Tim23	Cell Signaling	514463	1:500
Pyruvate dehydrogenase (PDH)	Cell Signaling	C54G1	1:1000
Carnitine palmitoyltransferase II (CPT2)	Abcam	18114	1:1000
Electron transfer flavoprotein subunit alpha (ETFA)	Sigma-Aldrich	HPA018990	1:1000

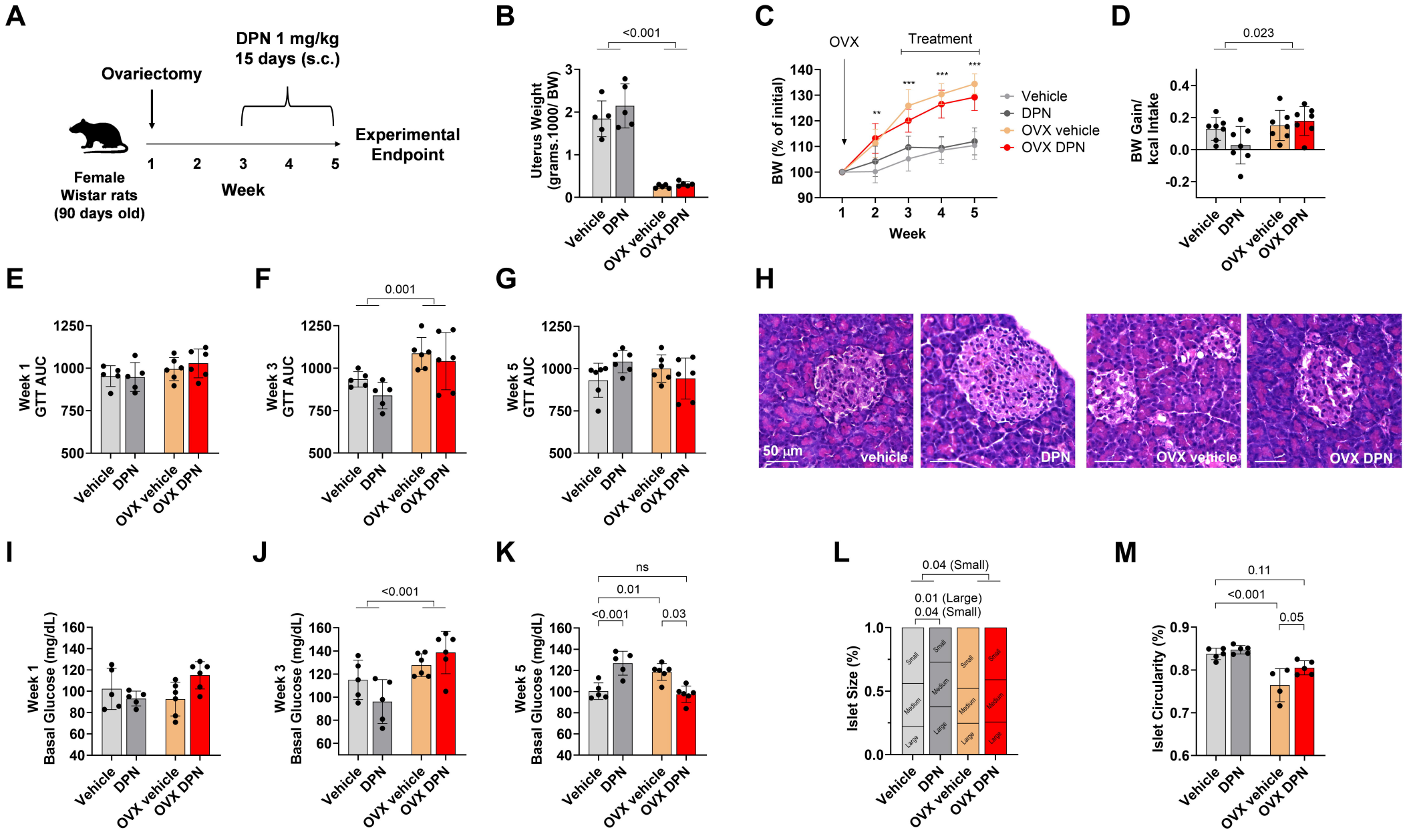
A
DPN 1 mg/kg
15 days (s.c.)
Ovariectomy
Experimental
Endpoint
Female
Wistar rats
(90 days old)
1
2
3
4
5
Week
B
<0.001
Uterus Weight
(grams.1000/ BW)
Vehicle
DPN
OVX vehicle
OVX DPN
C
OVX
Treatment
BW (% of initial)
Week
Vehicle
DPN
OVX vehicle
OVX DPN
D
0.023
BW Gain/
kcal Intake
E
Week 1
GTT AUC
F
0.001
Week 3
GTT AUC
G
Week 5
GTT AUC
H
50 µm
vehicle
DPN
OVX vehicle
OVX DPN
I
Week 1
Basal Glucose (mg/dL)
J
<0.001
Week 3
Basal Glucose (mg/dL)
K
ns
0.01
<0.001
0.03
Week 5
Basal Glucose (mg/dL)
L
0.04 (Small)
0.01 (Large)
0.04 (Small)
Islet Size (%)
Small
Medium
Large
M
0.11
<0.001
0.05
Islet Circularity (%)

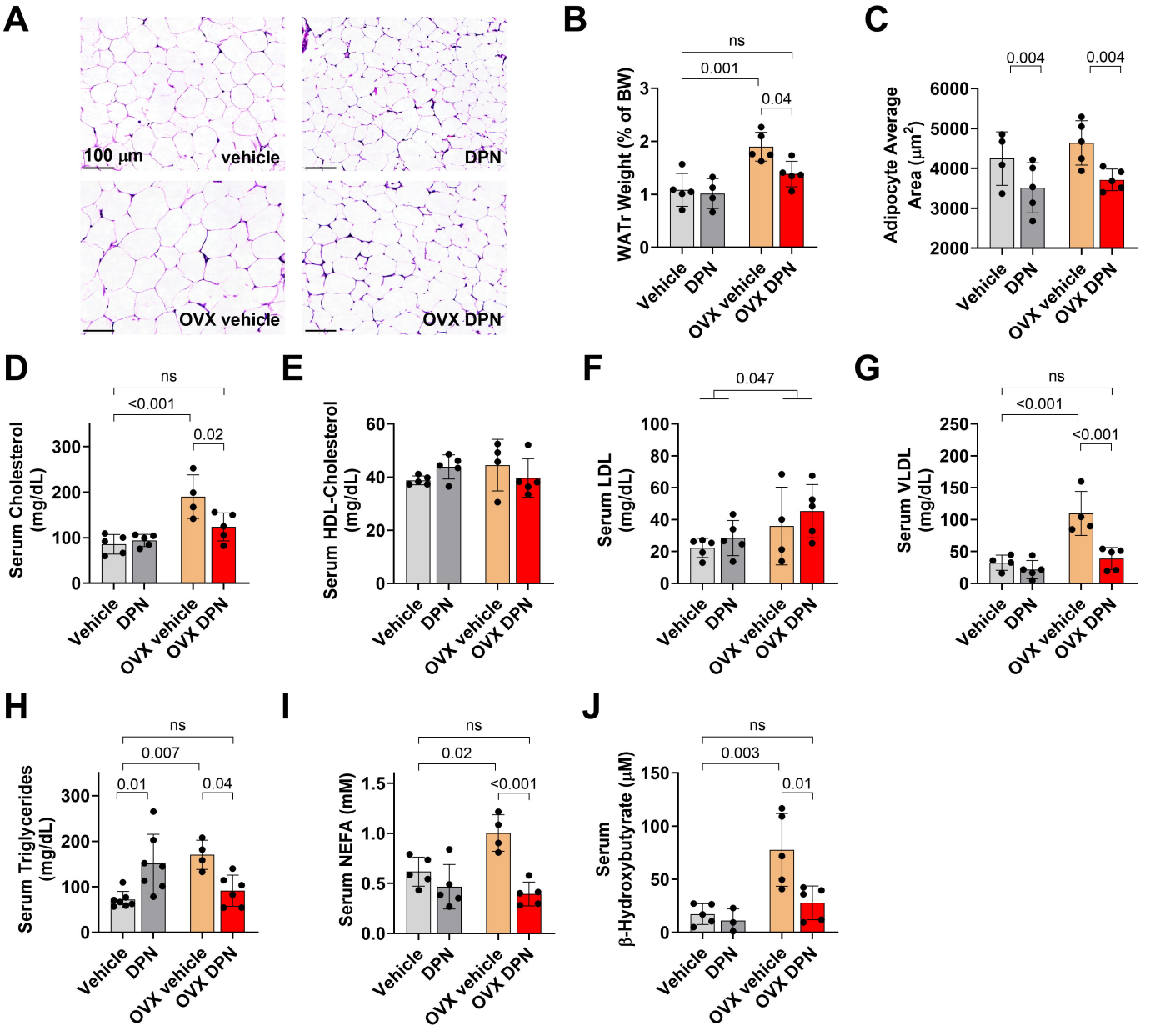
A
100 µm
vehicle
DPN
OVX vehicle
OVX DPN
B
WATr Weight (% of BW)
ns
0.001
0.04
Vehicle
DPN
OVX vehicle
OVX DPN
C
Adipocyte Average Area (µm²)
0.004
0.004
D
Serum Cholesterol (mg/dL)
ns
<0.001
0.02
E
Serum HDL-Cholesterol (mg/dL)
F
Serum LDL (mg/dL)
0.047
G
Serum VLDL (mg/dL)
ns
<0.001
<0.001
H
Serum Triglycerides (mg/dL)
ns
0.007
0.01
0.04
I
Serum NEFA (mM)
ns
0.02
<0.001
J
Serum β-Hydroxybutyrate (µM)
ns
0.003
0.01

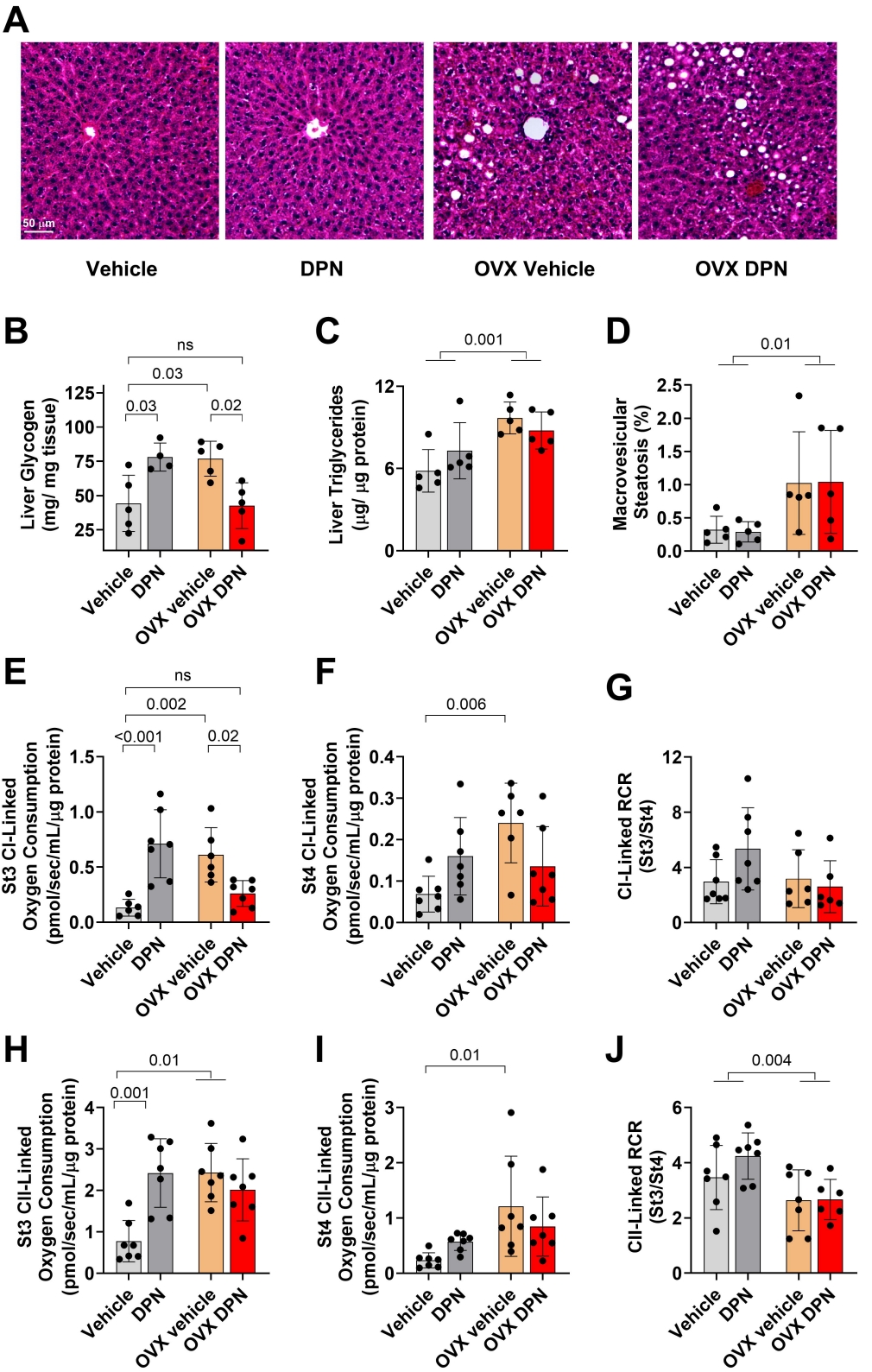
A
50 µm
Vehicle
DPN
OVX Vehicle
OVX DPN
B
Liver Glycogen (mg/ mg tissue)
ns
0.03
0.03
0.02
C
Liver Triglycerides (µg/ µg protein)
0.001
D
Macrovesicular Steatosis (%)
0.01
E
St3 CI-Linked Oxygen Consumption (pmol/sec/mL/µg protein)
ns
0.002
<0.001
0.02
F
St4 CI-Linked Oxygen Consumption (pmol/sec/mL/µg protein)
0.006
G
CI-Linked RCR (St3/St4)
H
St3 CII-Linked Oxygen Consumption (pmol/sec/mL/µg protein)
0.01
0.001
I
St4 CII-Linked Oxygen Consumption (pmol/sec/mL/µg protein)
0.01
J
CII-Linked RCR (St3/St4)
0.004
Vehicle
DPN
OVX vehicle
OVX DPN

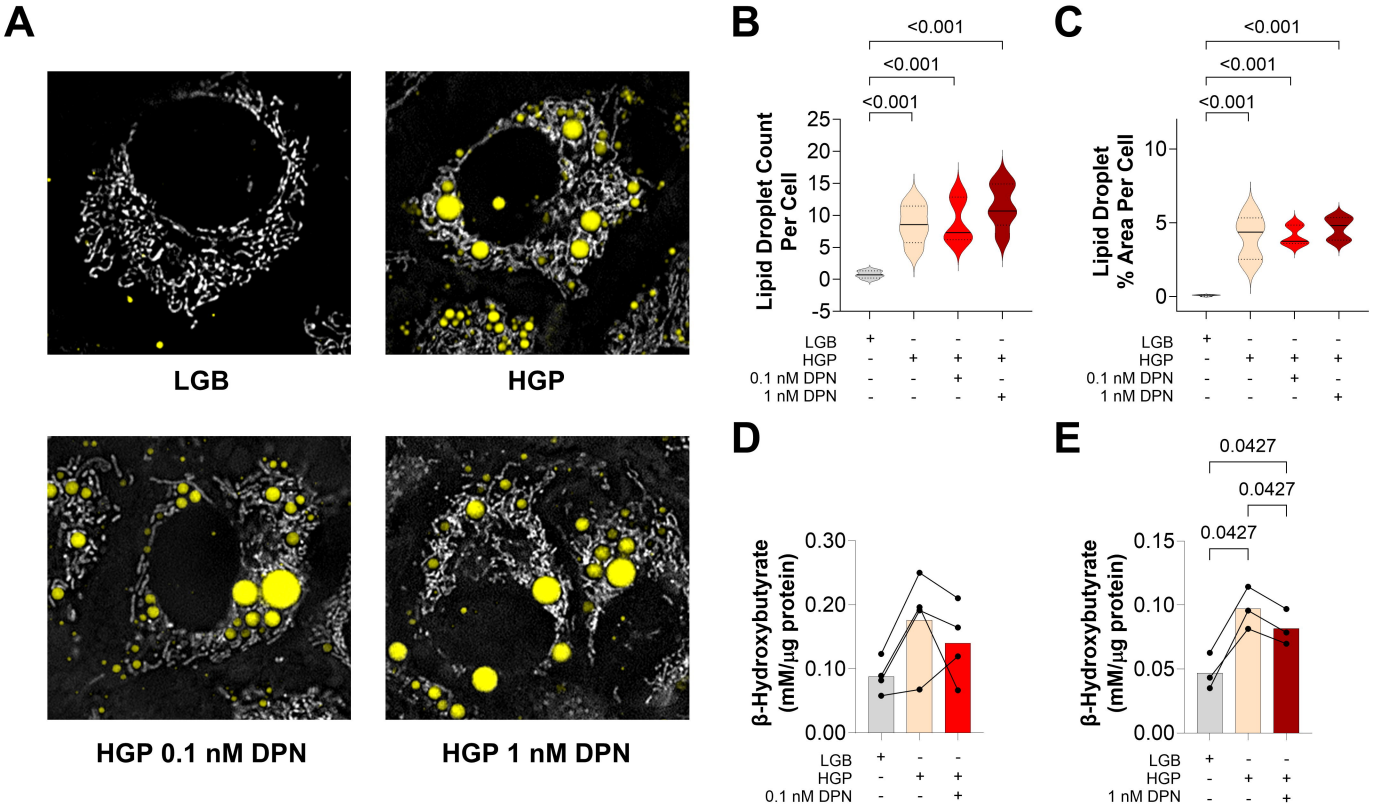
A
LGB
HGP
HGP 0.1 nM DPN
HGP 1 nM DPN
B
<0.001
<0.001
<0.001
Lipid Droplet Count Per Cell
25
20
15
10
5
0
-5
LGB + - - -
HGP - + + +
0.1 nM DPN - - + -
1 nM DPN - - - +
C
<0.001
<0.001
<0.001
Lipid Droplet % Area Per Cell
10
5
0
LGB + - - -
HGP - + + +
0.1 nM DPN - - + -
1 nM DPN - - - +
D
β-Hydroxybutyrate (mM/µg protein)
0.30
0.20
0.10
0.00
LGB + - -
HGP - + +
0.1 nM DPN - - +
E
0.0427
0.0427
0.0427
β-Hydroxybutyrate (mM/µg protein)
0.15
0.10
0.05
0.00
LGB + - -
HGP - + +
1 nM DPN - - +

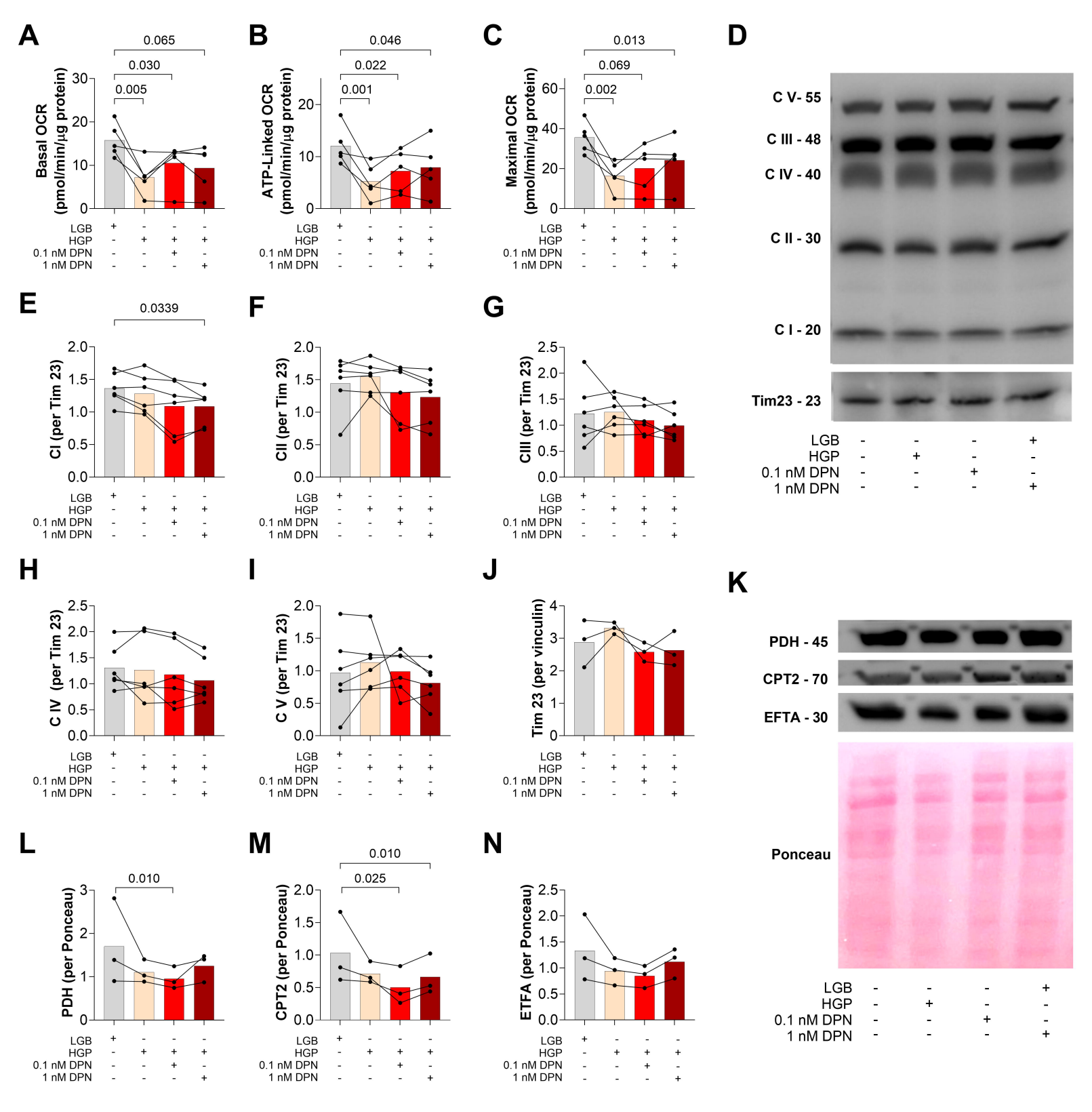
A
Basal OCR (pmol/min/µg protein)
0.065
0.030
0.005
B
ATP-Linked OCR (pmol/min/µg protein)
0.046
0.022
0.001
C
Maximal OCR (pmol/min/µg protein)
0.013
0.069
0.002
LGB
HGP
0.1 nM DPN
1 nM DPN
D
C V- 55
C III - 48
C IV - 40
C II - 30
C I - 20
Tim23 - 23
E
CI (per Tim 23)
0.0339
F
CII (per Tim 23)
G
CIII (per Tim 23)
H
C IV (per Tim 23)
I
C V (per Tim 23)
J
Tim 23 (per vinculin)
K
PDH - 45
CPT2 - 70
EFTA - 30
Ponceau
L
PDH (per Ponceau)
0.010
M
CPT2 (per Ponceau)
0.010
0.025
N
ETFA (per Ponceau)

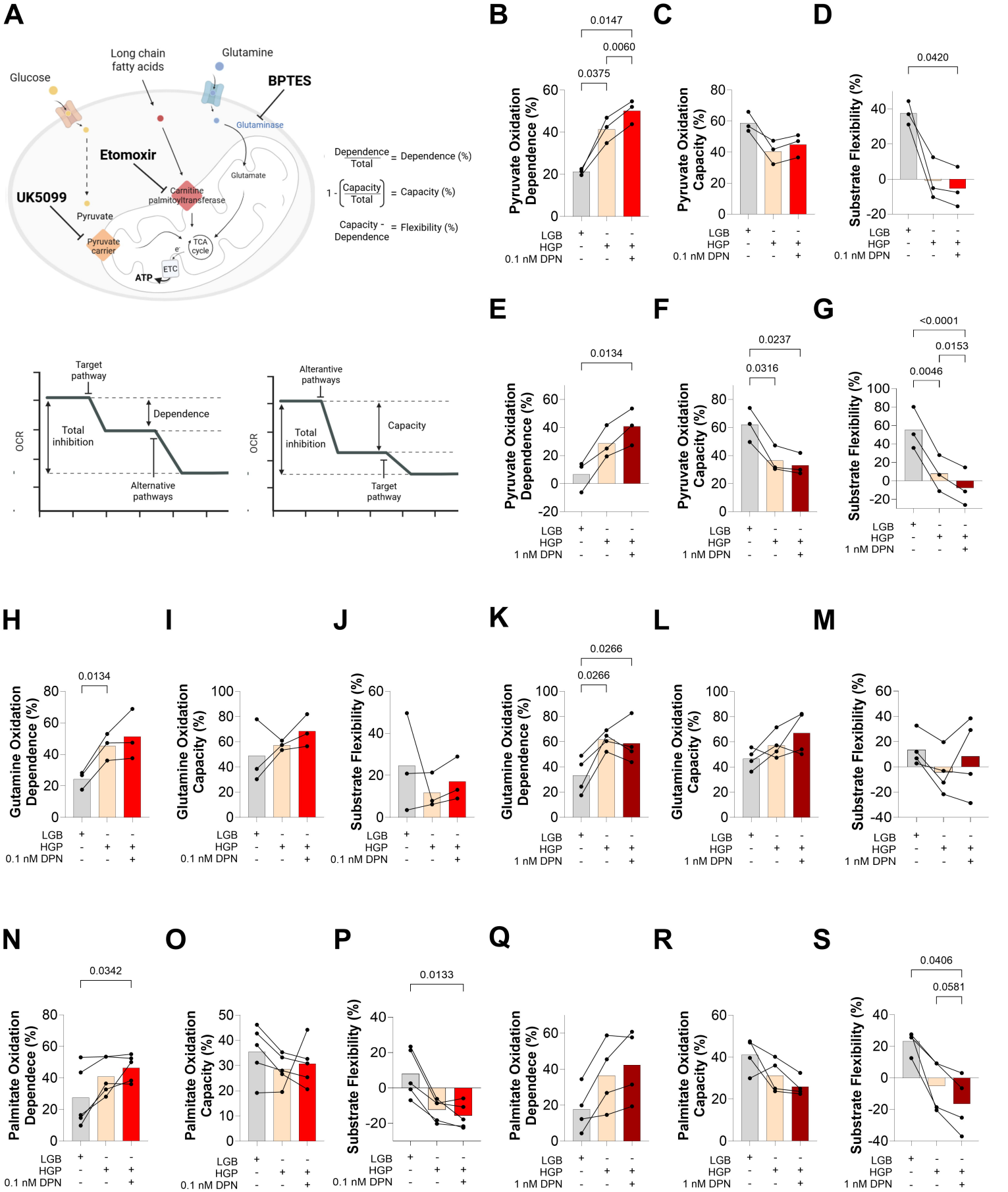
A
Glucose
Long chain fatty acids
Glutamine
BPTES
Glutaminase
Etomoxir
UK5099
Pyruvate
Pyruvate carrier
Carnitine palmitoyltransferase
Glutamate
TCA cycle
ETC
ATP
Dependence / Total = Dependence (%)
1 - (Capacity / Total) = Capacity (%)
Capacity - Dependence = Flexibility (%)
Target pathway
Dependence
Total inhibition
Alternative pathways
OCR
Alterantive pathways
Capacity
Target pathway
B
Pyruvate Oxidation Dependence (%)
0.0147
0.0060
0.0375
LGB
HGP
0.1 nM DPN
C
Pyruvate Oxidation Capacity (%)
D
Substrate Flexibility (%)
0.0420
E
Pyruvate Oxidation Dependence (%)
0.0134
1 nM DPN
F
Pyruvate Oxidation Capacity (%)
0.0237
0.0316
G
Substrate Flexibility (%)
<0.0001
0.0153
0.0046
H
Gutamine Oxidation Dependence (%)
0.0134
I
Glutamine Oxidation Capacity (%)
J
Substrate Flexibility (%)
K
Glutamine Oxidation Dependence (%)
0.0266
0.0266
L
Glutamine Oxidation Capacity (%)
M
Substrate Flexibility (%)
N
Palmitate Oxidation Dependece (%)
0.0342
O
Palmitate Oxidation Capacity (%)
P
Substrate Flexibility (%)
0.0133
Q
Palmitate Oxidation Dependece (%)
R
Palmitate Oxidation Capacity (%)
S
Substrate Flexibility (%)
0.0406
0.0581